Journal of
Ceramic Science
and Technology

J. Ceram. Sci. Technol., **16** [4] 255-261 (2025)
DOI: 10.4416/JCST2025-00007
available online at: http://www.ceramic-science.com

Additive Manufacturing of Lotus-Root-Inspired Honeycomb Ceramics: Implications for Oil/Water Separation and Cigar Smoke Filtration

Xiaokang Zhao[1], Hao Yin*[2,3], Pengfei Zhu*[3,4], Jing Che[1], Lei Han[1], Guangyuan Yang*[1], Congxin Chen[1]

[1]China Tobacco Hubei Industrial, LLC,Wuhan 430000, China.
[2]Chongqing University, Shapingba 174, Chongqing, China.
[3]FoShan (Southern China) Institute for New Materials, Foshan 528000, P. R. China.
[4]Shenzhen Adventure Tech Co. Ltd., Shenzhen 518053, PR China

received March 4, 2025; received in revised form June 17, 2025; accepted July 1, 2025

Abstract

In this study, lotus-root-inspired honeycomb alumina ceramics were fabricated using digital light processing (DLP) 3D printing technology, and a systematic investigation was conducted to determine the rheological characteristics of the alumina slurry and the mechanical properties of the sintered ceramics. Their potential applications in oil-water separation and cigar smoke filtration fields were explored. The experimental results showed that the viscosity of the 82 wt% Al_2O_3 ceramic slurry was 2 615 mPa·s at a shear rate of 30 s^{-1}, and the alumina ceramics sintered at 1 750 °C can resist high temperature with excellent mechanical properties: the three-point bending strength was 236 MPa, the compressive strength was 595 MPa, the Vickers hardness was 14.7 GPa, and the density was 3.77 g/cm³. In the oil-water separation experiment, the surface-modified honeycomb alumina ceramics were able to separate the oil-water mixture with high efficiency. When acting as one part of the cigar smoke filtration, the honeycomb ceramic provided support and sieved large particles out of the smoke. The filtration efficiencies for nicotine, total particulate matter, and tar reached 93.4 %, 91.7 %, and 89.7 %, respectively. In summary, high-performance honeycomb alumina ceramics were successfully prepared with 3D printing and showed broad application prospects in the separation field.

Keywords: Digital light processing, alumina ceramics, oil/water separation, cigar smoke filtration

I. Introduction

Porous ceramics combined the advantages of ceramic materials and honeycomb structure, and they were widely used in many fields [1], including tissue engineering [2], filtration [3], catalyst support [4], and thermal insulation [5]. This could be attributed to the outstanding properties of honeycomb ceramics, such as lightweight load bearing [6], high specific surface area characteristics [7], high thermal conductivity [8], and exceptional mechanical properties [9]. However, the high brittleness and hardness inherent in ceramic materials made it difficult to fabricate complex structural ceramic parts at low cost, severely limiting their applications [10]. Various methods have been adopted for molding honeycomb ceramics, such as gel casting [11], extrusion [12], freeze casting [13], and direct foaming [14]. However, each method had certain limitations in the process of manufacturing high-performance porous ceramics [15–18].

Recently, additive manufacturing (AM), also known as 3D printing, has been continuously developed in porous ceramic manufacturing [19]. It has enabled the fabrication of porous structures to be used in different applications under specific process conditions and in line with structural requirements, especially in the field of separation and catalysis, where customized porous structures were highly favored [20–23]. So far, various additive manufacturing techniques have been reported for the fabrication of honeycomb ceramic structures, such as direct ink writing (DIW) [24], selective laser sintering (SLS) [25], digital light processing (DLP) [26], stereolithography (SLA) [27], and 3D printing (3DP) [28]. DLP 3D printing technology has become one of the most popular 3D printing technologies for preparing ceramic parts owing to the fast molding speed, high printing accuracy, and wide range of molding materials [29]. Jin *et al.* [30] fabricated a gradient pore ceramic structure (GPCS) for high-efficiency oil-water separation, providing an efficient, simple, and reliable method for fabricating oil-water separation materials using 3D printing. Yao *et al.* [31] prepared high-performance hydroxyapatite ceramics using DLP 3D printing technology to achieve a triply periodic minimum surface (TPMS) structure to meet the requirements of cancellous bone substitutes. Wu *et al.* [32] investigated the effect of sintering additives on the properties of porous Si_3N_4 ceramics

* Corresponding author: gyyang100@126.com

prepared by DLP and laid an experimental foundation for controlling the properties of porous Si_3N_4 ceramics prepared by means of DLP. Therefore, the preparation of high-performance porous ceramics using DLP 3D printing held significant promise.

In addition, compared with metal materials, oxide-based ceramics with excellent chemical stability, corrosion and degradation resistance, excellent mechanical strength, and robust abrasion resistance were able to meet all the requirements for a robust and green solution with great chemical stability [33]. Therefore, it was feasible to use porous alumina ceramics in the field of separation.

In this study, honeycomb-structured alumina ceramics were skillfully fabricated by means of DLP 3D printing technology. An in-depth and meticulous investigation into the micromorphology and mechanical properties of the sintered porous alumina ceramics was carried out. Subsequently, the exploration of its applications in oil-water separation and cigar smoke filtration was launched (Fig. 1).

II. Materials and Methods

(1) Preparation of slurry

The photosensitive Al_2O_3 slurry for DLP printing was fabricated by mixing Al_2O_3 particles (D_{50} = 2.75 µm, Shenzhen Adventure Tech Co. Ltd, China) with photosensitive resin (ADT-Al_2O_3-TH01L, Shenzhen Adventure Tech Co. Ltd, China) that was composed of 3 wt% photoinitiator, 12.5 wt% dispersant, and 84.5 wt% acrylic resin, and then ball-milled for 6 h under 300 rpm with zirconia ball media in a planetary mill. The final solid loading of the slurry was controlled as 82 wt% (~ 56 vol%) with a viscosity of 2 615 mPa·s at 30 s^{-1}.

(2) Fabrication

Magics 21.0 software was used to design the porous alumina ceramic model. The model was then exported in the stereolithography (STL) format and imported into a 3D printer (ADT-3D-ZP-Priner-Pro-144 – 37.5, Shenzhen Adventure Tech Co. Ltd, China). The prepared slurry was poured into the printer, and the printing parameters were set. The surface power density in printing was 45 mW/cm^2. The exposure time for each layer and layer thickness were 3 s and 50 µm, respectively.

(3) Debinding and sintering

The preparation of honeycomb ceramics involves degreasing and sintering to remove the organic resin from the green body. The sample was placed in a muffle furnace (KSL-1200X-J, Hefei Ke Jing Materials Technology Co., Ltd., China) for debinding. First, the temperature was raised to 220 °C at a rate of 0.2 K/min and held for one hour. Then, the sample was heated to 500 °C at a rate of 0.14 K/min, and held at 360 °C and 500 °C for one hour each, to remove the residual organic matter and carbon residue. Finally, the temperature was increased to 1 750 °C at a rate of 5 K/min in a high-temperature furnace (BR-18M-1, Zhengzhou Brother Furnace Co. Ltd, China). After pressureless sintering at 1 750 °C for 2 h, sintered ceramic bodies were obtained (Fig. 2).

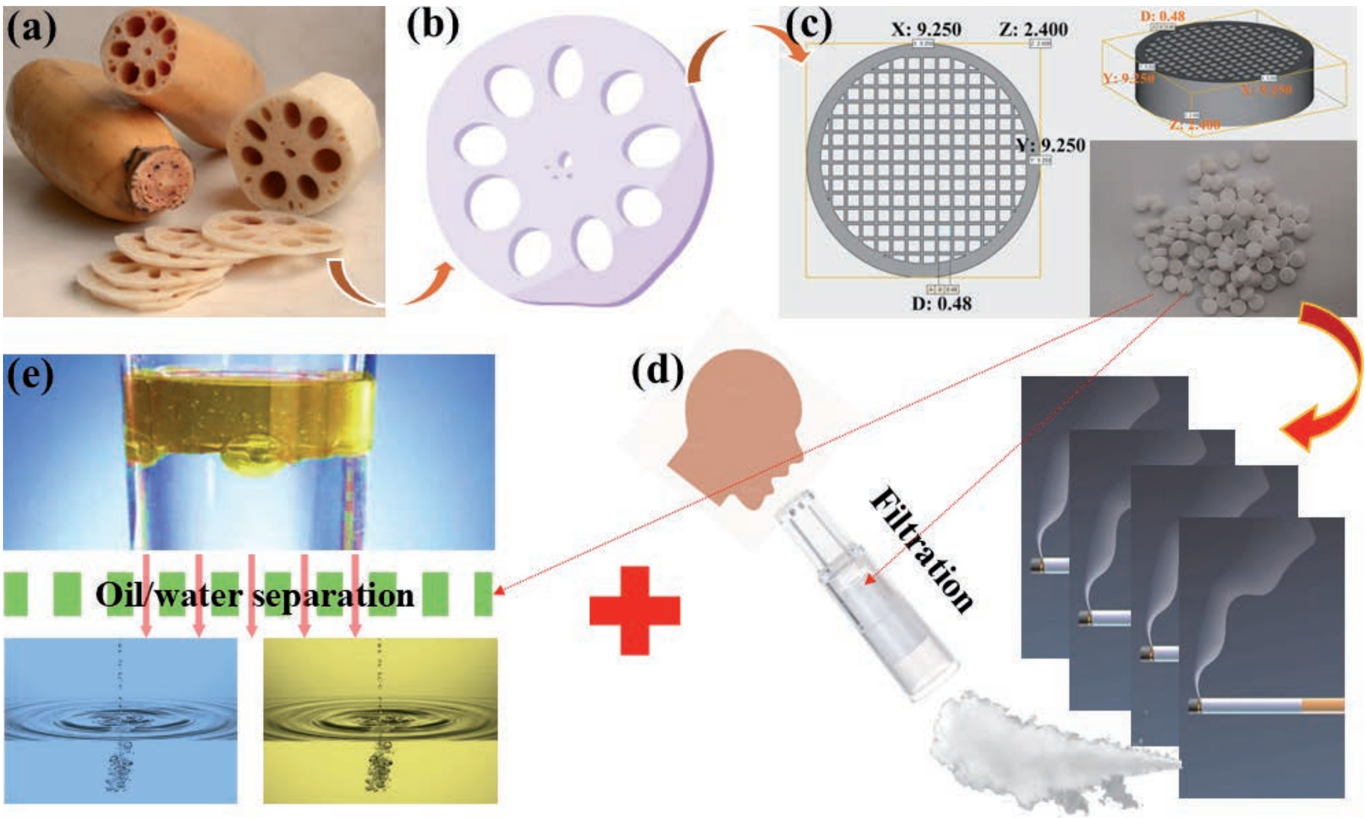

Fig. 1: Schematic diagrams showing the process of fabricating lotus-root-inspired honeycomb ceramics for cigar smoke filtration and oil/water separation.

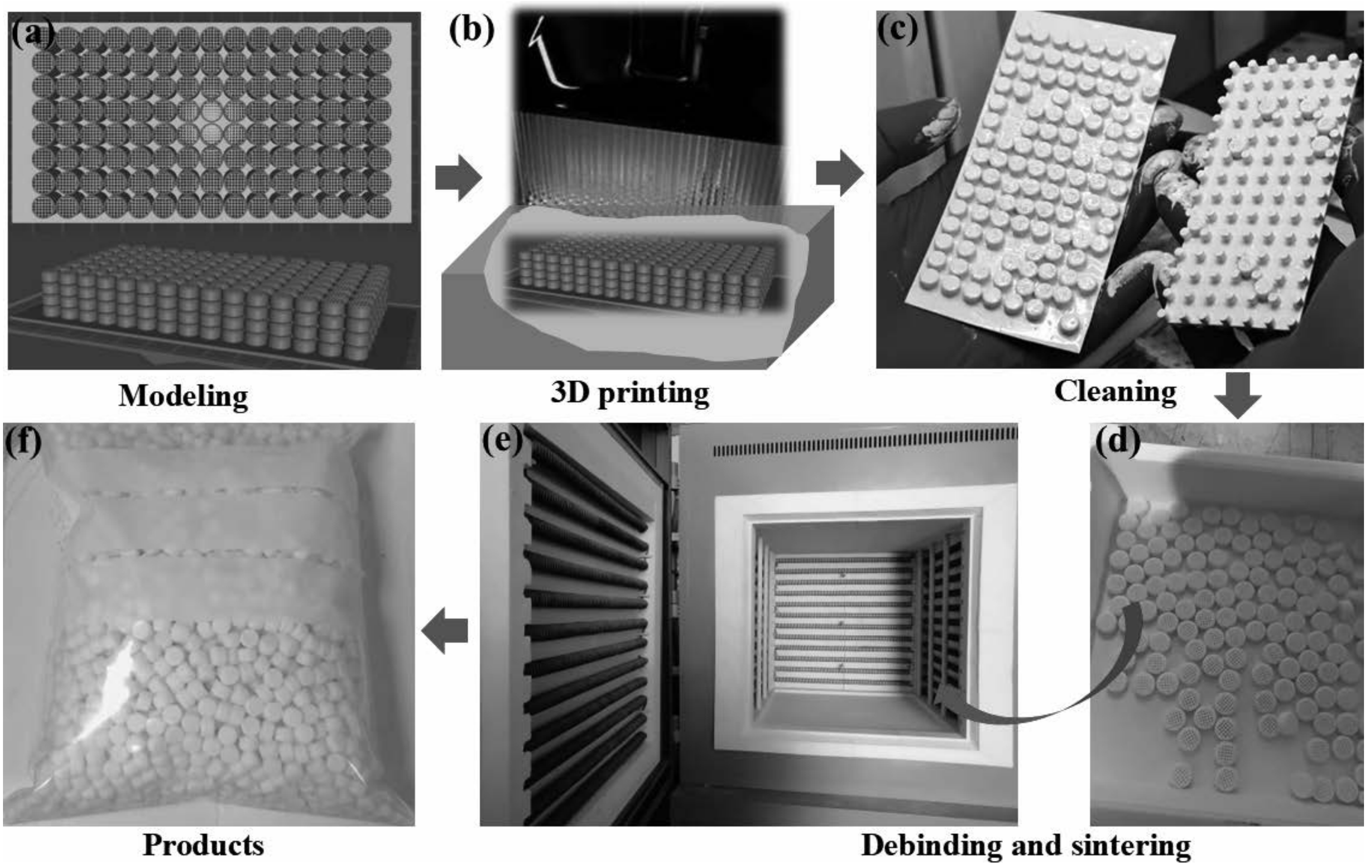

Fig. 2: Schematic diagrams showing the process of fabricating lotus-root-inspired honeycomb ceramics with DLP technology and subsequent sintering.

(4) Characterization

In this work, the rheological properties of the Al_2O_3 slurry were measured with a rotary rheometer (Thermofisher Ltd., Germany) at room temperature. Subsequently, the relative density and porosity of the alumina ceramics were determined using the Archimedes drainage method. The surface roughness of the ceramics was measured with an optical profilometer (ContourX-100, Bruker Corporation, USA). The bending and compressive strength of the Al_2O_3 porous ceramics were measured at a rate of 0.5 mm/min using a universal testing machine (GAX-5kNVD, SHIMADZU Co. Ltd, Japan). Finally, the microscopic morphology of the ceramic surface and cross-section after sintering was observed with a scanning electron microscope (Apreo2S, Thermo Fisher Scientific, USA).

III. Results and Discussions

DLP 3D printing was performed based on photosensitive resin-ceramic hybrid slurry, so it was important to study the rheological properties of slurry. Fig. 3a showed the results of the shear viscosity test of the ceramic slurry. It was found to have exhibited shear thinning characteristics, where the resin immobilized in the interstitial space of the ceramic powder was released as the shear rate increased, leading to a systematic alignment of the ceramic particles in the dynamic direction, which resulted in a decrease in viscosity. With a further increase in shear rate, the ceramic particles moved very close to each other. When a certain level was reached, the mutual collision and friction between particles increased and the viscosity rose. In the low shear rate region, the slurry exhibited high viscosity and a static state that supported the part. In the high shear rate region, the slurry was fluid and helped to spread the ceramic slurry on the printing platform. At a shear rate of 30 s^{-1}, the slurry viscosity was 2 615 mPa·s, which was less than 5 000 mPa·s and was suitable for light-curing 3D printing [34].

The mechanical properties of sintered ceramic samples were essential for practical applications. To test the mechanical properties of alumina ceramics fabricated with 82 wt% solid content slurry, samples sized 3 × 4 × 36 mm and 10 × 10 × 5 mm were prepared by means of DLP 3D printing and then sintered at 1 750 °C. Each set of experiments was repeated five times. Three-point bending and compressive strength tests were performed using a universal testing machine at room temperature. The bending and compressive strengths reached 236 MPa and 595 MPa, respectively. The Vickers microhardness was measured with a Vickers hardness tester, as presented in Fig. 3b. The Vickers hardness of the Al_2O_3 ceramic sample prepared from the 82 wt% content slurry was 14.7 GPa.

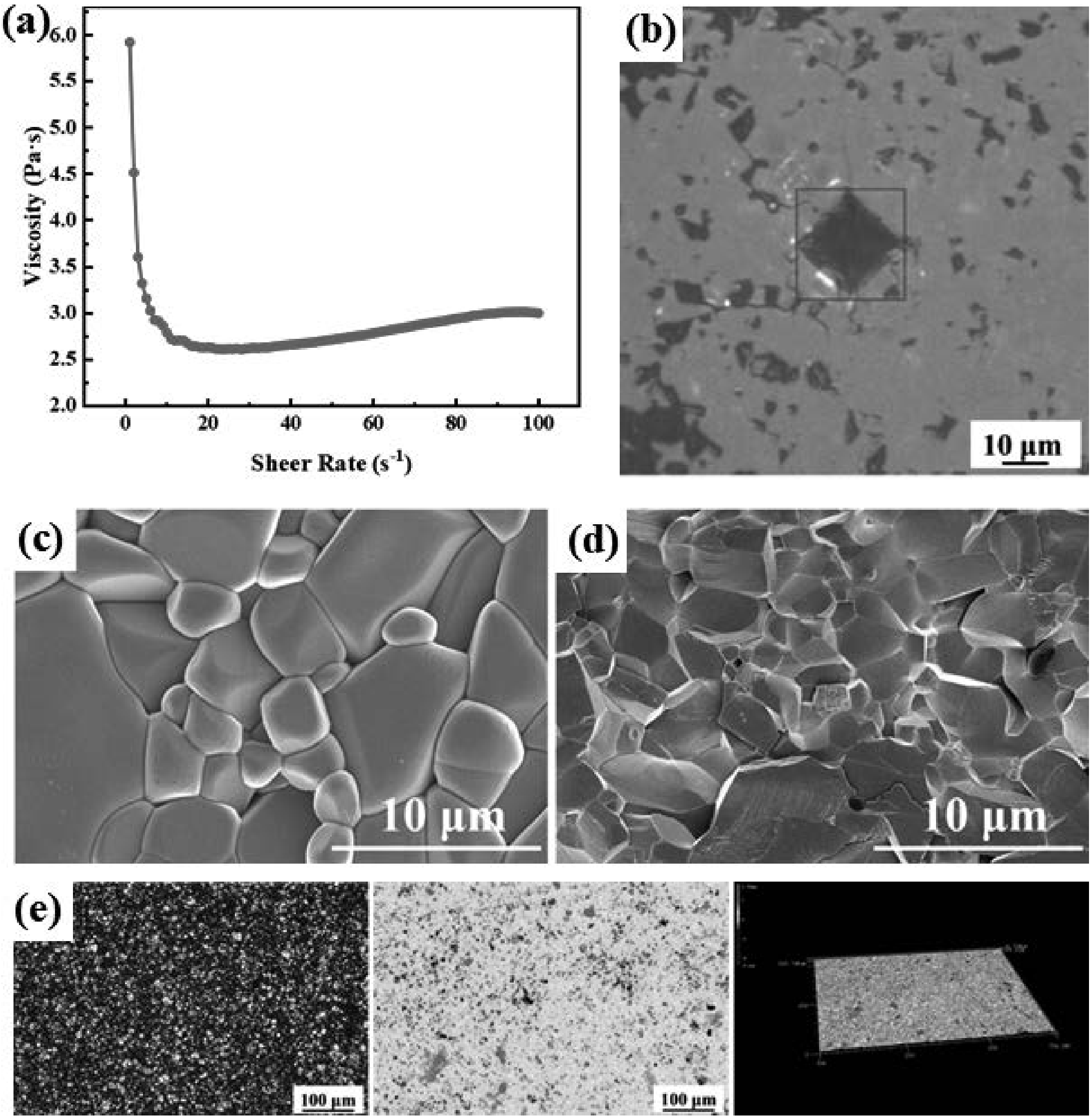

Fig. 3: Properties of photosensitive ceramic slurry and sintered ceramics. (a) Rheological properties of prepared alumina ceramic slurry (shear rate: 0 – 100 s^{-1}). (b) The sample surface after the Vickers microhardness test. (c) The surface morphology of sintered ceramic. (d) The cross-section morphology of sintered ceramic. (e) The surface roughness of sintered ceramics (0.75 µm).

Figs. 3c – d show the microscopic morphology of the ceramic surface and cross-section after sintering at 1 750 °C. It was clear that no defects such as delamination or cracks were observed inside the alumina ceramics. After sintering, the ceramic particles had been fused and no obvious boundaries between the particles were observed, indicating that the sintering densification process had been completed. Further observation of the section and surface made it difficult to capture the presence of pores. The closed porosity of the sample was 0.28 % and the density was 3.77 g/cm^3 as determined by Archimedes drainage method.

Finally, the application of sintered samples in the separation field was explored. First of all, the surface roughness of sintered ceramics was explored. As shown in Fig. 3e, the ceramic surface was rough, so it was not necessary to etch it to increase the surface roughness. As shown in Fig. 4, the surface was modified using n-Decyltriethoxysilane (DTES, 98 %), which was obtained from Alfa Aesar. Firstly, the sintered alumina samples were washed with ethanol and then dried naturally. Secondly, the silane solution was prepared by mixing DTES (25 vol%) in the IPA solution. The dried alumina sample was put into the silane solution overnight at room temperature. After that, it was rinsed with excessive IPA solution and cured at 70 °C for 3 – 5 hours. It was found that water droplets penetrated the surface of unmodified porous ceramics, but remained stable on the modified ceramic surface. Silanes were employed to alter the surface energy or wettability of substrates, without the intention of endowing the substrates with chemical reactivity. This process entailed self-condensation reactions within solvents after hydrolytic deposition onto the substrates, ultimately leading to the formation of siloxane bonds or silsesquioxane structures [35]. Through a systematic sequence of hydrolysis, condensation, hydrogen bonding, and finally bond formation, multiple planar layers were generated [36]. Hydrophobic hydrocarbon functional groups formed a hydrophobic layer on the ceramic surface. When the honeycomb ceramic was placed in water and then removed, it was found that all surfaces of the unmodified honeycomb ceramic had residual liquid, while the modified one remained clean. This was because an air film had been formed between the rough surface structure of the modified honeycomb ceramic and water. When the ceramic was immersed in an aqueous solution, liquid contact and contamination were prevented. These experimental results confirmed the stable self-cleaning ability of honeycomb ceramics and indirectly showed their excellent superhydrophobicity. To explore the oil-water separation performance of honeycomb ceramics, we fabricated honeycomb ceramics with a pore size of 500 µm. The separation device is presented in Fig. 5, where an oil-water mixture was gently introduced into the upper part of the device. The honeycomb ceramic could achieve oil-water separation as its rough structure and low surface energy gave rise to a significant capillary force. This capillary force enabled the selective permeation of the oil and water phases. This phenomenon could be elucidated based on the Young-Laplace theory. According to this well-established theory, the Young-Laplace equation was presented as follows [37]:

$$\Delta p = \frac{2\gamma \cos\theta}{r}$$

where Δp represented the additional pressure, specifically the pressure difference between the interior and exterior of the curved liquid surface (at the solid-liquid interface) of the adherent layer. γ stood for the surface tension of the liquid. θ denoted the contact angle, which characterized the interaction between the liquid and the solid surface. And r represented the pore diameter, a crucial geometric parameter influencing the relevant physical processes.

In addition to the application in the field of oil-water separation, porous ceramics also had notable applications in cigar smoke filtration. A filter was formed by combining porous ceramics and filter cotton, the structure of which is shown in Fig. 6. The results of the cigar smoke filtration test showed that it exhibited good cigar smoke filtration performance and could meet the requirements of cigar smoke filtration applications. This was because porous ceramics were prepared with a large number of evenly distributed and precisely sized pores. When the flue gas passed through the porous ceramics, the particles or molecules in the flue gas realized the separation based on the relationship between their size and the size of the ceramic pores. In addition, there were differences in the size and movement speed of different gas molecules in the flue gas. When they diffused in the pore space of the porous ceramic, their diffusion rates were different. Smaller molecules diffused relatively quickly and could pass through the porous ceramic more rapidly, while larger molecules diffused more slowly, thus achieving a certain degree of separation. The method T-115 (1999)

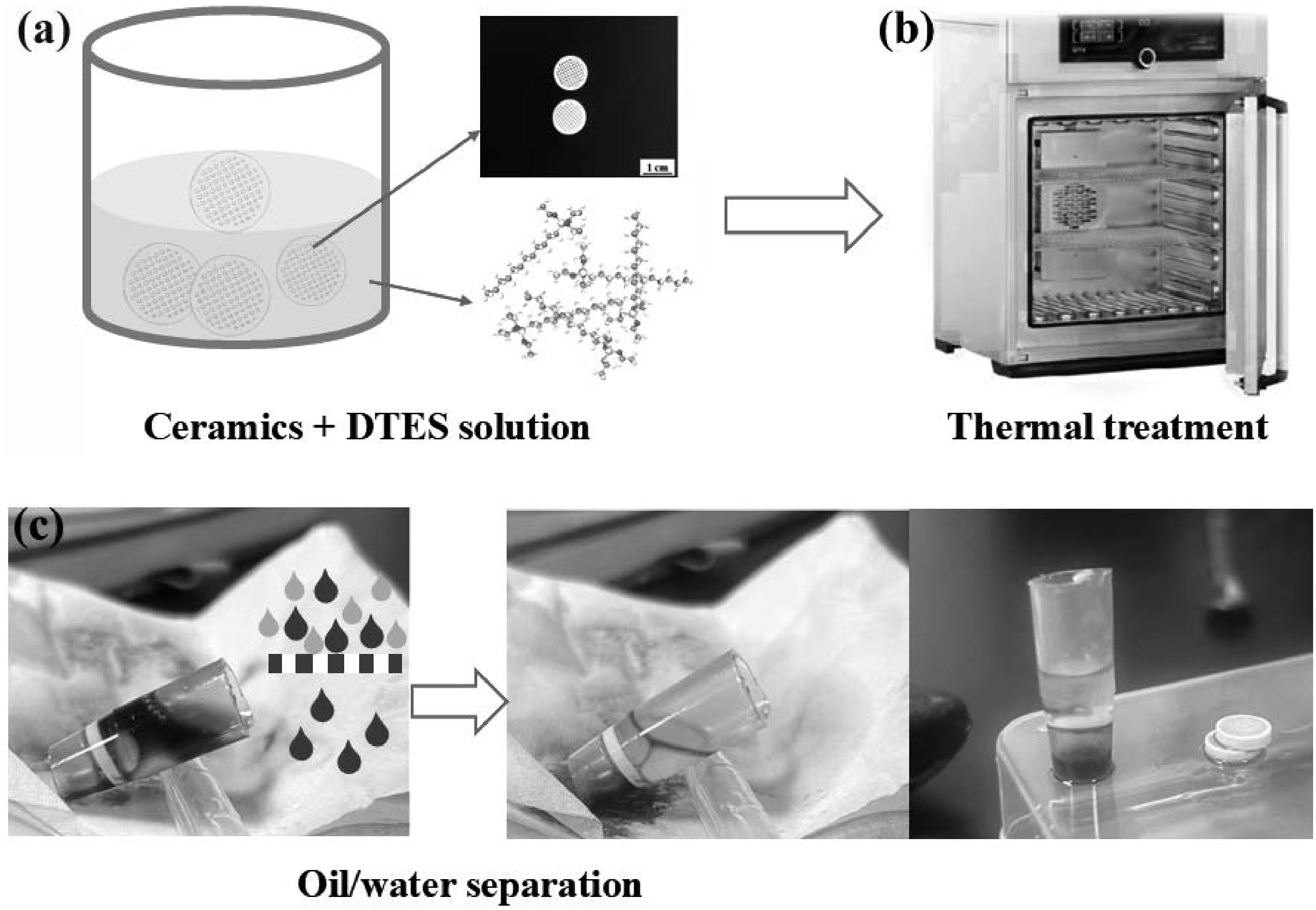

Fig. 4: (a) and (b) The process of coating ceramic surfaces with hydrophobic layers. (c) Digital image of separation device and oil-water mixture separation process.

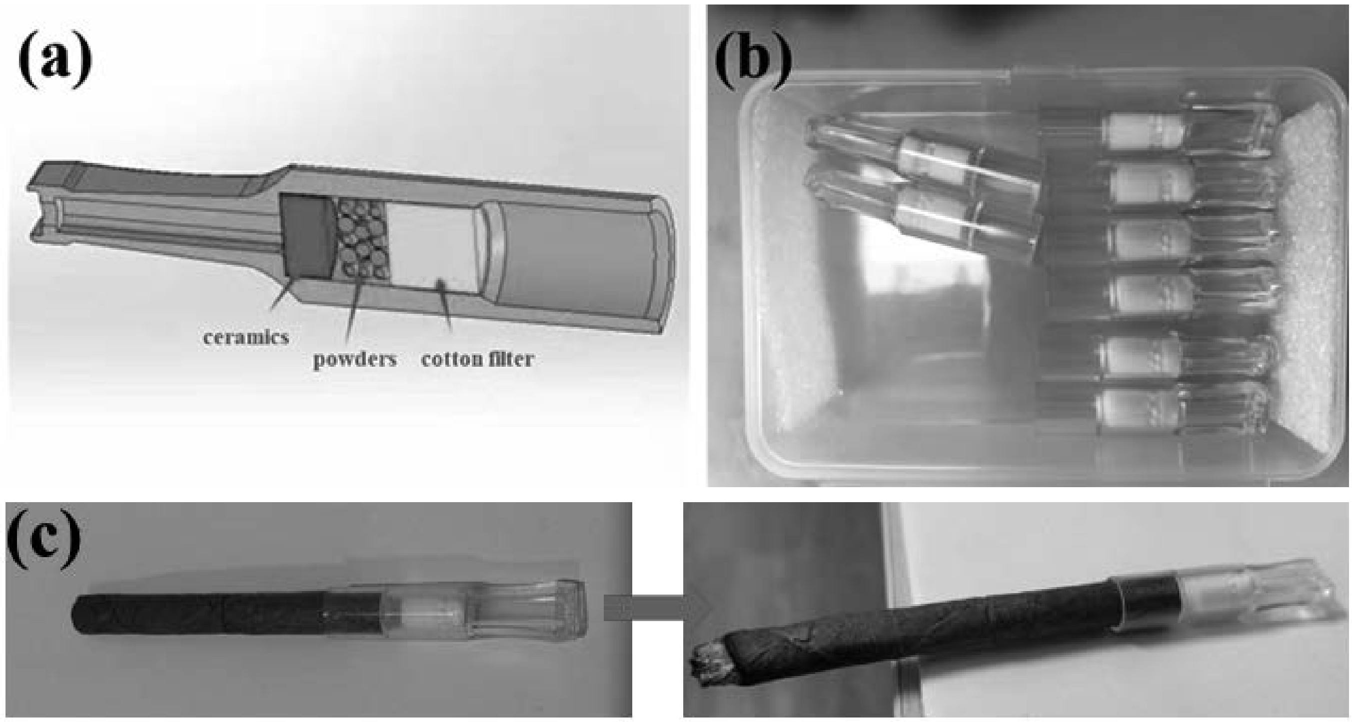

(d)

Items	Methods	Filtration efficiency
Nicotine		93.4
Particles	T-115(1999)	91.7
Tar		89.7
CO	C-QT-1930-TP	11.5

Fig. 5: (a) and (b) The cigar smoke filtration device. (c) Demonstration of use of the device for smoke filtration. (d) The filtration efficiency of the devices.

of Health Canada was used to test nicotine, total particulate matter, and tar in cigar samples. It was found that the filtration efficiency of the filter for nicotine, total particulate matter, and tar produced during the smoking process was 93.4 %, 91.7 %, and 89.7 %, respectively. The filter demonstrated good filtration performance and could reduce the inhalation of harmful substances. For a traditional filter cotton, commonly, the filtration efficiency tests yield different percentages. A specific test conducted by Zhou *et al.* showed that the removal efficiency for polycyclic aromatic hydrocarbons (PAHs) by the cotton and wool fibers reached 71.0 % (with absorption of up to 71.0 μg cig^{-1}) and 60.5 % (with absorption of up to 60.5 μg cig^{-1}), respectively [38]. The results for the products of this work showed better filtration performance than traditional filter cotton.

IV. Conclusions

This study was centered around honeycomb alumina ceramics fabricated by means of DLP 3D printing technology. A systematic exploration was carried out regarding the slurry characteristics, ceramic properties, and separation applications.

(1) It was found that the alumina ceramic slurry had shear thinning characteristics. At the shear rate of 30 s^{-1}, the slurry viscosity was 2 615 mPa·s.

(2) The 82 wt% alumina ceramics sintered at 1 750 °C had excellent properties. The density was 3.77 g/cm^3 and the porosity was only 0.28 %. In terms of mechanical properties, the three-point bending strength was 236 MPa, the compressive strength was 595 MPa, and the Vickers hardness was 14.7 GPa, showing good mechanical strength and hardness, which could meet the requirements of material mechanical properties in a variety of practical application scenarios.

(3) In the oil-water separation, the super-hydrophobicity of the sintered ceramic surface was significantly improved after modification. In the application of cigar smoke filtration, the filter made of porous ceramics and filter cotton exhibited filtering efficiency of 93.4 %, 91.7 % and 89.7 % for nicotine, total particulate matter and tar in flue gas, respectively.

References

1 Zhang, F. *et al.*: A review of 3D printed porous ceramics, *J. Eur. Ceram. Soc.,* **42**, 3351 – 3373, (2022).

2 Ma, H., Feng, C., Chang, J. & Wu, C.: 3D-printed bioceramic scaffolds: from bone tissue engineering to tumor therapy, *Acta Biomater.,* **79**, 37 – 59, (2018).

3 Jang, S. *et al.*: Digital light processing technique aided 3D printing hierarchical super-wetting mesh coated with hydrophobic SiO_2 for highly efficient oil-water separation. *J. Ind. Eng. Chem.,* **134**, 583 – 591, (2024).

4 Gong, H. *et al.*: Retrievable hierarchically porous ferroelectric ceramics for "Greening" the piezo-catalysis process, *Adv. Funct. Mater.*, **34**, 2311091, (2024).

5 Man, Y. *et al.*: A review on porous ceramics with hierarchical pore structure by 3D printing-based combined route, *J. Asian Ceram. Soc.*, **9**, 1377 – 1389, (2021).

6 Zhang, X. *et al.*: Additive manufacturing of cellular ceramic structures: from structure to structure-function integration, *Mater. Design*, **215**, 110470, (2022).

7 Al-Ketan, O., Soliman, A., AlQubaisi, A.M. & Abu Al-Rub, R.K.: Nature-inspired lightweight cellular co-continuous composites with architected periodic gyroidal structures, *Adv. Eng. Mater.*, **20**, 1700549, (2018).

8 Chen, Y. *et al.*: Review on porous ceramic-based form-stable phase change Materials: preparation, enhance thermal conductivity, and application, *ChemBioEng Reviews*, **10**, 941 – 958, (2023).

9 Huang, K., Zhong, K., Liu, Z., Wang, F. & Hu, S.: Direct ink writing of non-sintered ceramic with biomimetic cellular structure, *Ceram. Int.*, **50**, 41711 – 41721, (2024).

10 Tabard, L. *et al.*: Robocasting of highly porous ceramics scaffolds with hierarchized porosity, *Additive Manufacturing*, **38**, 101776, (2021).

11 Deng, X. *et al.*: Foam-gelcasting preparation of high-strength self-reinforced porous mullite ceramics, *J. Eur. Ceram. Soc.*, **37**, 4059 – 4066, (2017).

12 Liang, D. *et al.*: Influencing factors on the performance of tubular ceramic membrane supports prepared by extrusion, *Ceram. Int.*, **47**, 10464 – 10477, (2021).

13 Dang, W. *et al.*: Freeze-cast porous Al_2O_3 ceramics strengthened by up to 80% ceramics fibers, *Ceram. Int.*, **48**, 9835 – 9841, (2022).

14 Du, Z. *et al.*: The high porosity silicon nitride foams prepared by the direct foaming method. *Ceram. Int.*, **45**, 2124 – 2130, (2019).

15 Luo, X., Zhang, Q., Ye, F. & Cheng, L.: Microstructure, mechanical, wave-transparent and heat insulation properties of Si_3N4 foam ceramic by organic foam impregnation combined with CVI, *J. Mater. Res. Tech*., **23**, 1332 – 1346, (2023).

16 Stochero, N.P. *et al.* Ceramic shell foams produced by direct foaming and gelcasting of proteins: Permeability and microstructural characterization by X-ray microtomography, *J. Eur. Ceram. Soc.,* **40**, 4224 – 4231, (2020).

17 Salleh, S.Z. *et al.*: Recycling food, agricultural, and industrial wastes as pore-forming agents for sustainable porous ceramic production: A review, *J. Clean. Prod.*, **306**, 127264, (2021).

18 Zhou, W., Zhang, Z., Li, N., Yan, W. & Ye, G.: A new mullite foamed ceramic prepared by direct-foaming methods in parallel with a mechanical activation technique, *Ceram. Int.*, **48**, 20721 – 20730, (2022).

19 Feng, C. *et al.*: Additive manufacturing of hydroxyapatite bioceramic scaffolds: dispersion, digital light processing, sintering, mechanical properties, and biocompatibility, *J. Adv. Ceram.,* **9**, 360 – 373, (2020).

20 Jin, Z. *et al.*: High-strength, superhydrophilic/underwater superoleophobic multifunctional ceramics for high efficiency oil-water separation and water purification, *Mater. Today Nano*, **18**, 100199, (2022).

21 Tijing, L.D. *et al.*: 3D printing for membrane separation, desalination and water treatment, *Appl. Mater. Today*, **18**, 100486, (2020).

22 Zoumpouli, G.A., Guaraldo, T.T., Warren, Z., Mattia, D. & Chew, J.: Reimagining the shape of porous tubular ceramics using 3D printing, *Appl. Mater. Today*, **37**, 102136, (2024).

23 Wu, S. *et al.*: Coaxial 3D printed Al_2O_3 ceramic continuous-flow fixed-bed reactor with bionic core-shell structure, *Ceram. Int.*, **50**, 13662 – 13670, (2024).

24 Liu, Q. & Zhai, W.: Hierarchical porous ceramics with distinctive microstructures by emulsion-based direct ink writing, *ACS Appl. Mater. Inter.*, **14**, 32196 – 32205, (2022).

25 Sun, X. *et al.*: 3D printing of porous SiC ceramics added with SiO_2 hollow microspheres, *Ceram. Int.*, **46**, 22797 – 22804, (2020).

26 Tian, C. *et al.*: Effect of polystyrene addition on properties of porous Si_3N4 ceramics fabricated by digital light processing, *Ceram. Int.*, **49**, 27040 – 27049, (2023).

27 Li, S., Bao, C., Liu, R. & Dong, W.: Using anisotropy rationally to fabricate porous cordierite ceramic with enhanced mechanical properties based on supportless stereolithography, *Mater. Sci. Eng. A*, **891**, 146000, (2024).

28 Zhou, Z. *et al.*: Development of three-dimensional printing polymer-ceramic scaffolds with enhanced compressive properties and tuneable resorption, *Mater. Sci. Eng. C*, **93**, 975 – 986, (2018).

29 Wu, H. *et al.*: Vat photopolymerization of silicon carbide strengthened alumina ceramic composites with honeycomb structure for heat insulation and oil/water separation, *Ceram. Int.*, **50**, 31504 – 31518, (2024).

30 Jin, Z. *et al.*: 3D-printed controllable gradient pore super-wetting structures for high temperature efficient oil-water separation, *J. Materiomics*, **7**, 8 – 18, (2021).

31 Yao, Y. *et al.*: High performance hydroxyapatite ceramics and a triply periodic minimum surface structure fabricated by digital light processing 3D printing, *J. Adv. Ceram.*, **10**, 39 – 48, (2021).

32 Wu, Y.-R. *et al.*: Influence of the ratio of sintering aids on the properties of porous Si_3N4 ceramics fabricated by digital light processing, *Ceram. Int.,* **49**, 33004 – 33010, (2023).

33 Echeverria Aparicio, I., Fishpool, D.T., Rubio Diaz, V., Dorey, R.A. & Yeomans, J.A.: Evaluation of polymer matrix composite manufacturing routes for production of an oxide/oxide ceramic matrix composite, *J. Eur. Ceram. Soc.*, **42**, 2420 – 2428. (2022).

34 Hinczewski, C., Corbel, S. & Chartier, T.: Stereolithography for the fabrication of ceramic three- dimensional parts, *Rapid Prototyping J.*, **4**, 104 – 111, (1998).

35 Antonucci, J.M., Dickens, S.H., Fowler, B O. & Xu, H.H.K.: Chemistry of silanes: interfaces in dental polymers and composites, *J. Res. Natl. Inst. Stand. Technol.*, **110**, 541, (2005).

36 Jonhson, W. *et al.*: 3D-printed hierarchical ceramic architectures for ultrafast emulsion treatment and simultaneous Oil-Water filtration, *ACS Materials Lett.*, **4**, 740 – 750, (2022).

37 Ge, J., Wang, F., Yin, X., Yu, J. & Ding, B.: Polybenzoxazine-functionalized melamine sponges with enhanced selective capillarity for efficient oil spill cleanup, *ACS Appl. Mater. Interfaces,* **10**, 40274 – 40285, (2018).

38 Zhou, S., Fu, Z., Xia, L., *et al.*: Blocking and filtering effect of filter tips of natural fibers against mainstream cigarettes smoke[J], *J. Nat. Fibers*, **18,** 2327 – 2337, (2021).